

MIMO with More Users than RF Chains

Nil Garcia, *Member, IEEE*, Henk Wymeersch, *Member, IEEE*, Erik G. Larsson, *Fellow, IEEE*

Abstract—Antenna arrays with hybrid analog-digital signal processing capabilities offer a compromise between the performance of digital arrays and the cost-efficiency of analog arrays with a single radio-frequency (RF) chain. A limitation of hybrid arrays is that the number of independent streams that they can transmit with standard precoding techniques cannot be larger than the number of RF chains. In standard hybrid precoding, the analog precoder (phase shifters or switches) are fixed at the beginning of the streams. To break the ceiling on the number of streams, a new precoding paradigm is proposed, where the analog and digital precoder are changed in a symbol-by-symbol basis. Algorithms for optimizing the analog and digital precoders at the symbol rate are provided and their performance is extensively analyzed.

I. INTRODUCTION

Multi-user multiple-input multiple-output (MU-MIMO) systems are expected to play a pivotal role in the fifth generation (5G) of wireless networks [1]. 4G cellular systems and its long-term-evolution (LTE) already used small MIMO on base stations (BS) or terminals but limited to a few antennas. Instead, 5G base stations (BS) are expected to equip massive MIMO stations with far more antennas than active users per time-frequency slot, perhaps in the order of hundreds or even more. The benefits of massive MIMO have been studied intensively and include, but are not limited to, enormous spectral efficiency boost, channel hardening and lower inter-user interference (IUI) [2].

Altogether with massive MIMO, moving to the millimeter wave (mm-Wave) spectrum is another key enabler for 5G because the colossal portions of underutilized bandwidth shall enable speeds in the order of Gbps [3], [4]. Current CMOS technology is mature enough to work at mm-Wave; however, massive MIMO still faces some problems at such high frequencies: high power consumption and high installation cost [5]. To address these shortcomings, hybrid analog-digital architectures, where the number of radio-frequency (RF) chains is much smaller than the number of antennas, have been identified as a potential remedy. The main idea is to shift some of the digital baseband processing towards the analog frontend. Typically, in a hybrid array each RF chains is routed to set of antennas through phase shifters. Some more novel hybrid architectures are also possible utilizing switches in place of phase shifters [6], or even lenses as the entire analog frontend [7].

N. Garcia and H. Wymeersch are with the Department of Electrical Engineering, Chalmers University of Technology, Gothenburg, Sweden. E. G. Larsson is with the Division of Communication Systems, Department of Electrical Engineering (ISY), Linköping University, Linköping, Sweden. This research was supported in part, by the EU HIGHTS project (High precision positioning for cooperative ITS applications) MG-3.5a-2014-636537, the VINNOVA COPPLAR project, funded under Strategic Vehicle Research and Innovation grant No. 2015-04849, the Swedish Research Council (VR) and ELLIIT

Precoding in hybrid arrays is a combination of analog and digital precoding. The analog precoder (e.g., phase shifters) is tuned at the beginning of the data stream, while the digital precoding occurs just before transmitting the symbols through the RF chains. Consequently, the number of independent transmitted streams (and so the maximum number of users served) in a time-frequency slot is restricted to the number of RF chains [8]–[10]. While hybrid massive arrays offer advantages such as low user interference, the ceiling on the number of streams implies that the achievable sum rate and spectral efficiency is lower than that of a digital array [11]. In order to serve more users than RF chains quasi simultaneously, in [12] the phase shifters of a purely analog array are adjusted in symbol-by-symbol basis, such that they steer energy towards a different user at each consecutive symbol. Effectively they manage to serve multiple users at the cost of a diminished user rate due to the time multiplexing. Another interesting approach is that of [13] where they manage to transmit as many streams as RF chains plus one by employing spatial modulation. By turning on and off some of the transmit antennas, an extra stream of data can be conveyed to the receiver without an extra RF chain.

In this work we propose a hybrid precoding strategy which enables transmitting more streams than RF chains are available. Contrary to standard hybrid precoding, the analog and digital precoders are, both, changed in a symbol-by-symbol basis. The main idea is that by jointly optimizing the analog and digital precoders for each transmission, we can approximate any precoder much better than if they are fixed for the entire duration of the stream. Hence, we term such scheme symbol-by-symbol (SbS) hybrid precoding. To achieve successful SbS precoding, we develop some algorithms which generate any arbitrary precoder vector with the hybrid array with a small error. In turn, we show numerically that the error difference between the ideal precoder and the hybrid approximation decreases exponentially with the number of RF chains, and therefore, our strategy allows the hybrid array to effectively behave as a purely digital array. However, the cost of this strategy is that the analog and digital precoders need to be recomputed at the symbol rate.

The proposed algorithms for performing SbS hybrid precoding are improved versions of previous techniques [14]–[17] based on Orthogonal Matching Pursuit (OMP) which is a well established tool from compressive sensing. However, contrary to previous works which had to rely on approximations of OMP, we show that it is possible to compute OMP exactly and efficiently for the case of a hybrid architecture with phase shifters or switches. In addition to studying the performance of SbS hybrid precoding, we also analyze its defects, such as spectral regrowth created by performing constant phase shifting or switching and the distortion caused by such non-

linear precoding strategy.

II. MORE DOWNLINK STREAMS THAN RF CHAINS

A common assumption in MIMO communications is that the number of transmitted streams cannot be larger than the number of RF chains available at the transmitter [8]–[10]. While in sub-6 GHz frequencies this is not an impediment because arrays usually have as many RF chains as antennas, in higher frequencies such as mm-Wave each RF chain is very costly. In this section, a solution is proposed which effectively allows hybrid arrays to act as a purely digital arrays in the downlink, thus, enabling many more streams than RF chains, and also more sophisticated precoding strategies.

Assume a multi-user-MIMO (MU-MIMO) setup where a base station (BS) is equipped with a large-scale array transmitting K streams for K users. Let $s_{k,t}$ be the transmitted symbol of the k -th stream at discrete time t , with average power $\mathbb{E}|s_{k,t}|^2 = P$. The streams are zero-mean and independent so that $\mathbb{E}s_{k,t}s_{k',t}^* = 0$ for $k \neq k'$. Then, the transmitted signal across all N antennas is

$$\mathbf{y}_t = \mathbf{F}\mathbf{s}_t, \quad (1)$$

where $\mathbf{s}_t = [s_{1,t} \ \cdots \ s_{K,t}]^T$ and \mathbf{F} is the precoding matrix of size $N \times K$ normalized to $\|\mathbf{F}\|_F = 1$. The k -th user receives the signal

$$z_{k,t} = \mathbf{h}_k^T \mathbf{y}_t = \mathbf{h}_k^T \mathbf{F}\mathbf{s}_t + n_{k,t}, \quad (2)$$

where \mathbf{h}_k is the channel matrix and the noise $n_{k,t} \sim \mathcal{CN}(0, P_n)$. If a user has multiple antennas, we assume that it combines the received signal all antennas linearly such it is often the case in mm-Wave; and therefore, it is equivalently modeled as a single-antenna user with the gain of the combiner as part of the channel. Upon defining the channel matrix as $\mathbf{H} = [\mathbf{h}_1 \ \cdots \ \mathbf{h}_K]^T$, the vector of samples collectively received at the K users is given by

$$\mathbf{z}_t = \mathbf{H}\mathbf{F}\mathbf{s}_t + \mathbf{n}_t. \quad (3)$$

A. Hybrid Analog-Digital Precoding

Let L be the number for RF chains at the BS. Contrary to arrays with full digital processing, analog-digital precoders are constrained to a specific set depending on the hybrid architecture. This work assumes a hybrid architecture, portrayed in Fig. 1, where each RF chain is routed to each antenna through a phase shifter or switch, and for this reason it is called a fully connected network. A more detailed description of this hybrid architecture is provided in [6] under the name A2 and A4 depending on whether it uses phase shifters or switches. The switching network is a more novel concept and it has been barely studied to the best of the authors knowledge, whereas the same architecture based on phase shifters is quite popular in the literature [5], [18], [19]. This fully connected network is considered to be more costly compared to other hybrid alternatives because it requires NL phase shifters or switches. However, as it will be shown in the next section, it has the untapped potential of virtually behaving as a purely digital

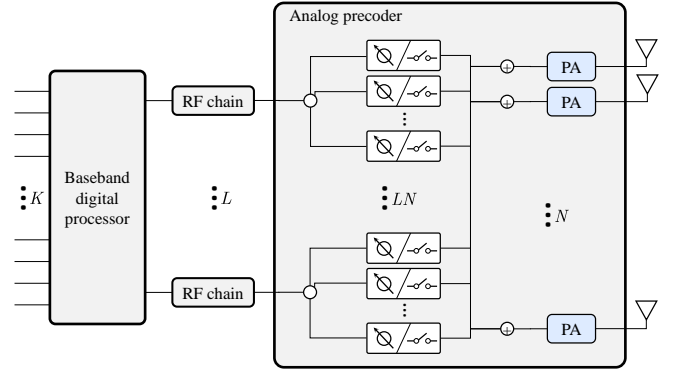


Fig. 1. Transmitter with analog-digital precoding. The radio frequency (RF) chains are routed to all antennas through a mesh of phase shifters or switches. The number of RF chains is usually much smaller than the number of antennas. PA stands for power amplifier.

array. Mathematically, the precoders for the hybrid architecture can be modeled as

$$\mathbf{F} = \mathbf{F}_{\text{RF}}\mathbf{F}_{\text{BB}}, \quad (4)$$

where \mathbf{F}_{RF} and \mathbf{F}_{BB} are implemented on the RF/analog and BB/digital domain, respectively. Let \mathcal{B} represent the set of discrete phase shifts $\mathcal{B} = \{1, e^{i2\pi/Q}, \dots, e^{i2\pi(Q-1)/Q}\}$ in the case of a phase shifting network, or on/off states $\mathcal{B} = \{0, 1\}$ for a switching network; then, the entries of \mathbf{F}_{RF} are constraint to $\mathbf{F}_{\text{RF}} \in \mathcal{B}^{N \times L}$, whereas the digital precoder $\mathbf{F}_{\text{BB}} \in \mathbb{C}^{L \times K}$. Since the rank of \mathbf{F} can be at most L , the maximum number of linearly independent streams that can be transmitted is $K \leq L$. In the limit case of a single RF chain $L = 1$, then the beamforming becomes purely analog and the array is only capable of transmitting a single stream $K = 1$. For the case of a purely digital array $\mathbf{F} = \mathbf{F}_{\text{BB}} \in \mathbb{C}^{N \times K}$ and the number of independent streams is N . In addition, choosing \mathbf{F}_{RF} is non trivial for most cases because, irrespective of the metric of choice, it involves optimizing over discrete variables for which the global minimum cannot be computed efficiently [10], [20], [21].

B. Linear Precoding

Linear precoding is extremely popular in downlink MU-MIMO because of its simplicity and good performance [22], [23]. Next, we review two of the most popular techniques: maximum-ratio-transmission (MRT) and zero-forcing (ZF). MRT works best when the arrays are large and the channel is composed of a few paths because the large aperture produces very narrow beams which result in little inter-user interference. MRT's formula is given by [24]

$$\mathbf{F} \propto \mathbf{H}^H \quad (5)$$

up to a normalization factor. Another popular precoding scheme is zero forcing (ZF) which essentially tries to cancel out all interference between users and whose formula is [24]

$$\mathbf{F} \propto \mathbf{H}^H(\mathbf{H}\mathbf{H}^H)^{-1} \quad (6)$$

While in sub 6 GHz frequencies, ZF precoding and its derivatives are quite popular; in millimeter MRT is usually a

more preferred choice because all entries of \mathbf{F} have constant amplitude and can be easily implemented with analog phase shifters.

Note that both of these simple techniques cannot be implemented with a hybrid array if the number of RF chains is lower than the number of users because $\text{rank} \mathbf{F} < L$ and $\text{rank} \mathbf{H} = K$. In fact, even if there are enough RF chains, due to the constraints on the structure of the analog precoder, there may not exist a pair of analog and digital precoders (4) equal to the MRT or ZF precoders.

C. Symbol-by-Symbol Hybrid Precoding

To break the ceiling on the number of streams $K \leq L$, we propose a symbol-by-symbol (SbS) precoding approach instead where the analog and digital precoders are changed, as the name suggest, on a symbol-by-symbol basis. To achieve this, it is necessary that the phase shifters and switches change their state in less than a symbol period. This is currently possible with state-of-the-art phase shifters and switches which change their state in less than a few hundred pico seconds [25]–[28]. A similar idea is that of [12] where a beam is steered towards a different user at every symbol period by performing ultra fast phase shifting. Since we assume a narrow-band model (array response independent of the frequency), in order to satisfy the condition ‘bandwidth much smaller than carrier frequency’, then, at mm-Wave frequencies, the symbol period must be approximately larger than a 1 ns. Thus, in practice the phase shifters and switches operations can be regarded almost as instantaneous.

The main idea behind SbS precoding is to change the analog and digital precoders at each symbol period such that it transmits the same signal as if we had an ideal linear precoder (1), i.e.,

$$\mathbf{F}\mathbf{s}_t \approx \mathbf{F}_{\text{RF}}^t \mathbf{f}_{\text{BB}}^t, \quad (7)$$

for all t . Matrix \mathbf{F}_{RF}^t represents the phase shifts or switches, and \mathbf{f}_{BB}^t the inputs to the RF chains. Our hypothesis is that a pair $\mathbf{F}_{\text{RF}}^t \in \mathcal{B}^{N \times L}$ and $\mathbf{f}_{\text{BB}}^t \in \mathbb{C}^{L \times 1}$ exists such that (7) holds accurately even for $K > L$ for all t . An obvious way to cast the problem of estimating the SbS precoders is a least squares fit

$$\min_{\substack{\mathbf{F}_{\text{RF}}^t \in \mathcal{B}^{N \times L} \\ \mathbf{f}_{\text{BB}}^t \in \mathbb{C}^{L \times 1}}} \|\mathbf{F}\mathbf{s}_t - \mathbf{F}_{\text{RF}}^t \mathbf{f}_{\text{BB}}^t\|_2. \quad (8)$$

If the obtained solution is close to zero, then it is quasi-optimal since zero is a trivial lower-bound. Nonetheless, the challenges to solving (8) are numerous:

- A) Due to \mathbf{F}_{RF}^t , the optimization problem (8) involves discrete variables for which, in general, the global optimum cannot be retrieved efficiently.
- B) Also, since this problem needs to be solved at each transmission t , the solver must enjoy low computational complexity even when the number of antennas grows very large.
- C) Condition (7) needs to hold for the entire duration of the stream.

- D) Finally, the sharp transitions caused by the phase shifters/switches may distort the signal in the time domain and produce spectral regrowth.

The next section proposes some algorithms for accurate and fast SbS precoding and their performance is evaluated numerically in Section IV.

III. SBS PRECODING WITH ORTHOGONAL MATCHING PURSUIT

A. General Approach

The ideal target precoder at time t is $\mathbf{y}_t = \mathbf{F}\mathbf{s}_t$. To avoid overloading the notation, the subindex t is dropped from hereon. Solving the mixed discrete-continuous optimization problem (8) is challenging. An alternative approach [29] is to recast it as a sparse recovery problem

$$\min_{\mathbf{x}} \|\mathbf{y} - \Phi \mathbf{x}\|_2 \quad (9a)$$

$$\text{s.t. } \|\mathbf{x}\|_0 \leq L, \quad (9b)$$

where $\|\cdot\|_0$ counts the number of non-zero entries, \mathbf{x} is an L -sparse vector, and the dictionary Φ is built by concatenating all column vectors $\mathbf{a} \in \mathcal{B}^N$. Assume \mathbf{x} is the global optimum, then \mathbf{f}^{BB} is obtained by subtracting the L non-zero entries of \mathbf{x} , and \mathbf{F}_{RF} is formed by selecting the columns of Φ with the same indexes than the L non-zeros. In the above sparse setting, vector \mathbf{x} can then be recovered using compressive sensing tools. Because sparse problems are NP-hard, retrieval of the global optimum is not guaranteed but they can lead to good suboptimal solutions. As in previous works [14]–[17], [29], [30], we rely on orthogonal matching pursuit (OMP) [31] to solve (9) whose pseudocode is presented in Algorithm 1. OMP

Algorithm 1 Orthogonal matching pursuit

inputs: \mathbf{y} and L

outputs: \mathbf{F}_{RF} and \mathbf{f}^{BB}

1: initialize $\mathbf{r} = \mathbf{y}$

2: **for** $l = 1, \dots, L$ **do**

3: solve

$$\hat{\mathbf{a}} = \arg \min_{\alpha \in \mathbb{C}, \mathbf{a} \in \mathcal{B}^N} \|\mathbf{r} - \alpha \mathbf{a}\|_2$$

4: $\mathbf{F}_{\text{RF}} \leftarrow [\mathbf{F}_{\text{RF}} \quad \hat{\mathbf{a}}]$ (first iteration \mathbf{F}_{RF} is empty)

5: $\mathbf{f}^{\text{BB}} = (\mathbf{F}_{\text{RF}}^H \mathbf{F}_{\text{RF}})^{-1} \mathbf{F}_{\text{RF}}^H \mathbf{y}$

6: $\mathbf{r} = \mathbf{y} - \mathbf{F}_{\text{RF}} \mathbf{f}^{\text{BB}}$

7: **end for**

is a popular greedy approach where one column of \mathbf{F}_{RF} is estimated at a time. The optimum value of α in step 3 has the closed form expression $\alpha = \mathbf{a}^H \mathbf{r} / \|\mathbf{a}\|_2^2$. By plugging it back and performing some basic algebra, we find that line 3 can also be expressed as

$$\hat{\mathbf{a}} = \arg \max_{\mathbf{a} \in \mathcal{B}^N} \frac{|\mathbf{a}^H \mathbf{r}|}{\|\mathbf{a}\|_2}. \quad (10)$$

This is in fact the standard method for computing step 3 when the dictionary is arbitrary, and its computational complexity is $\mathcal{O}(C)$ where C is the number of columns in the dictionary [32]. However, in this case, the number of columns grows

exponentially as $C = |\mathcal{B}|^N$. To deal with the exponentially growing dictionary, most of the existing approaches restricted themselves to a subset of columns of Φ ; thus, yielding degraded performance. Instead we show in the next sections that this step can be computed exactly with polynomial complexity, for the phase shifting and switching networks, by taking into account the structure of the dictionary. The result of applying OMP exactly is a vast improvement in performance as illustrated in Section IV.

B. Phase Shifting Network

We aim at solving (10) exactly and efficiently when $\mathcal{B} = \{1, e^{i2\pi/Q}, \dots, e^{i2\pi(Q-1)/Q}\}$. The number of states of a phase shifter is $Q = 2^B$ where B is the number of control bits, and the phase shifters' resolution is $\delta = 2\pi/Q$. It turns out that this problem is equivalent to the problem of multiple-symbol differential detection in communications for which an algorithm was proposed [33], [34] for solving this problem exactly with polynomial complexity. Its detailed steps are in Algorithm 2 and for the proofs refer to the original paper [33]. In each iteration of the loop in Algorithm 2, only lines 5–8 are

Algorithm 2 Optimal phase shifts

inputs: \mathbf{r} and δ

outputs: \mathbf{a}

- 1: let Ω be a permutation such that $\text{mod}(\angle r_{\Omega(1)}, \delta) \leq \dots \leq \text{mod}(\angle r_{\Omega(N)}, \delta)$
 - 2: set $z_n = |r_{\Omega(n)}|e^{i \text{mod}(\angle r_{\Omega(n)}, \delta)}$ for $n = 1, \dots, N$
 - 3: initialize $S = \sum_{n=1}^N z_n$ and $v = 0$
 - 4: **for** $m = 1, \dots, N$ **do**
 - 5: **if** $|S| > v$ **then**
 - 6: $v = |S|$ and $m_{\text{opt}} = m$
 - 7: **end if**
 - 8: $S \leftarrow S - z_m + z_m e^{i\delta}$
 - 9: **end for**
 - 10: $a_{\Omega(n)} = \begin{cases} e^{i(\angle r_{\Omega(n)} - \angle z_n - \delta)} & n = 1, \dots, m_{\text{opt}} - 1 \\ e^{i(\angle r_{\Omega(n)} - \angle z_n)} & n = m_{\text{opt}}, \dots, N \end{cases}$
-

executed and they scale linearly with the number of antennas N . However, the sorting in line 1 has complexity $\mathcal{O}(N \log N)$. Back in Algorithm 1, the next most costly operations after line 3 are lines 5 and 6, whose complexity when performing the matrix products from right to left is also linear with N . Thus, the OMP method can be computed exactly with complexity $\mathcal{O}(N \log N)$.

C. Switching Network

The fully connected hybrid architecture based on switches is particularly interesting because its power consumption is much lower than its phase shifting alternative [6]. A switch has only two states, open/closed, and can be modeled by the binary set $\mathcal{B} = \{0, 1\}$. We aim at computing line 3 of Algorithm 1,

$$\min_{\substack{\alpha \in \mathbb{C} \\ \mathbf{a} \in \mathcal{B}^N}} \|\mathbf{r} - \alpha \mathbf{a}\|_2, \quad (11)$$

efficiently. The naive/exhaustive approach to this problem where all possible values of $\mathbf{a} \in \mathcal{B}^N$ are tested and then α

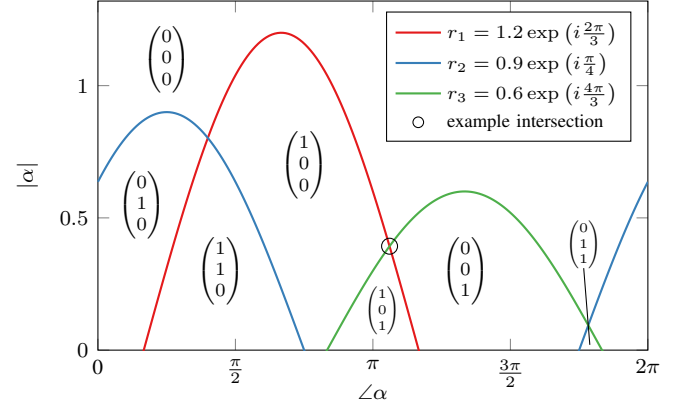


Fig. 2. Plot of $|\alpha| = 2|r_n|\cos(\angle\alpha - \angle r_n)$ for $n = 1, 2, 3$. Each region is labeled with the locally optimal \mathbf{a} obtained by (12). From the figure we can infer that $\mathbf{a} = [1, 1, 1]^T$ is not the solution because it does not belong to any region. To find the global optimum, we would need to plug all values of \mathbf{a} shown in the figure (all combinations except $[1, 1, 1]^T$) into (10). While the improvement of this procedure in terms of computational cost is similar to the exhaustive approach for very small N , it is much faster for large N .

is computed by least squares has complexity $\mathcal{O}(2^N)$. In this section we propose a procedure that scales as $\mathcal{O}(N^2)$.

If α in (11) was fixed and known, then $a_n = 1$ if $|r_n - \alpha| < |r_n|$, $a_n = 0$ if $|r_n - \alpha| > |r_n|$, and a_n is undetermined (in the sense that 0 and 1 are both optimal) when equality holds. Define $\angle z$ as the phase of z . By squaring and performing basic algebraic manipulations, the condition simplifies to

$$a_n = \begin{cases} 1 & \text{if } |\alpha| < 2|r_n|\cos(\angle\alpha - \angle r_n) \\ 0 \text{ or } 1 & \text{if } |\alpha| = 2|r_n|\cos(\angle\alpha - \angle r_n) \\ 0 & \text{else,} \end{cases} \quad (12)$$

for $n = 1, \dots, N$. Thus, from this perspective, $\mathbf{a} \triangleq \mathbf{a}(\alpha)$ and (11) boils down to a search over the magnitude and phase of α . By plotting the boundaries, for which a_n transitions from 0 to 1 for all n , on a two-dimensional plane with coordinates $|\alpha|$ and $\angle\alpha$, the plane is partitioned into multiple regions associated with different locally optimal solutions of \mathbf{a} . See Fig. 2 for an example with only $N = 3$ components. All boundaries are scaled and shifted copies of a truncated cosine, and therefore any two boundaries will intersect. Since the global optimum must belong to one of these regions, first we find \mathbf{a} for each region, and then evaluate which is the best through (10).

To find the local optimal \mathbf{a} of each region, it suffices to find any point $(|\alpha|, \angle\alpha)$ within each region and then apply (12) to obtain the local optimal \mathbf{a} . Since all regions' boundaries include at least an intersection point, a simple strategy is to collect all intersection points by solving the two-equation system

$$|\alpha| = 2|r_m|\cos(\angle\alpha - \angle r_m) \quad (13)$$

$$|\alpha| = 2|r_k|\cos(\angle\alpha - \angle r_k) \quad (14)$$

for all $m \neq k$, and whose solutions turn out to be

$$(|\alpha|, \angle\alpha) \in \left\{ \left(2\Re r_m e^{-i[\angle(r_m - r_k) \pm \frac{\pi}{2}]}, \angle(r_m - r_k) \pm \frac{\pi}{2} \right) : m, k = 1, \dots, N \text{ and } m \neq k \right\}. \quad (15)$$

From (15), it is obvious that there are at most N^2 different intersection points. Also, from (12) we know that for α at the intersection of the m -th and k -th curve, the optimal values of a_n and a_m can be 0 or 1. This coincides with the notion that the intersection points limit with four different regions associated to four different \mathbf{a} . Thus, to ensure we collect the local optima \mathbf{a} of all regions, we compute \mathbf{a} with (12) for each value of α in (15) and generate all four possible combinations $(a_m, a_k) = (0, 0), (0, 1), (1, 0), (1, 1)$ in order to obtain a set of locally optima \mathbf{a} :

$$\mathcal{F} = \left\{ \mathbf{a} : a_n = \begin{cases} c_1 & \text{if } n = m \\ c_2 & \text{else if } n = k \\ 1 & \text{else if } \Im[(r_n - r_m)(r_m - r_k)^*] \leq 0 \\ 0 & \text{else} \end{cases} \right. \quad (16)$$

$$\left. m, k = 1, \dots, N \text{ and } m \neq k \text{ and } c_1, c_2 = 0, 1 \right\}.$$

Contrary to the original feasible set \mathcal{B}^N which grows exponentially with the number of antennas, the new set (16) grows quadratically with the number of antennas N . At last, the global optimum \mathbf{a} is obtained by exhaustively evaluating all points in (16) with (10). Algorithm 3 summarizes the steps of the proposed solution.

Algorithm 3 Optimal on/off states

inputs: \mathbf{r}

outputs: \mathbf{a}

- 1: compute \mathcal{F} with (16)
 - 2: initialize $v_{\text{opt}} = 0$
 - 3: **for** $\mathbf{w} \in \mathcal{F}$ **do**
 - 4: $v = \|\mathbf{w}^H \mathbf{r}\| / \|\mathbf{w}\|$
 - 5: **if** $v > v_{\text{opt}}$ **then**
 - 6: $v_{\text{opt}} = v$
 - 7: $\mathbf{a} = \mathbf{w}$
 - 8: **end if**
 - 9: **end for**
-

Set \mathcal{F} grows quadratically with N , and in addition, each iteration in the loop of Algorithm 3 requires performing operations over vectors of length N . Thus, the computational complexity of Algorithm 3, and consequently of Algorithm 1, is $\mathcal{O}(N^3)$.

D. Distortion in SbS Hybrid Precoding

In terms of the received signal at all users, the problem with SbS hybrid precoding is that the approximation (7) will in general not be exact (see Section IV-A for numerical evidence). Since this approximation changes in a symbol-by-symbol basis, the actual received signal by the k -th user (2), even in the absence of noise, will not be an exact scaled replica

of the transmitted streams $\{s_{k,t}\}_{k=1}^K$. Instead, the received signal by the k -th user may be expressed as

$$z_{k,t} = \mathbf{h}_k^T \mathbf{F}_{\text{RF}}^t \mathbf{f}_{\text{BB}}^t \triangleq \sum_{k'=1}^K g_{k,k'} s_{k',t} + d_{k,t} + n_{k,t}, \quad (17)$$

where $g_{k,k}$ is a scaling factor (gain), $g_{k,k'}$ is the interference from user k' to user k , and $d_{k,t}$ accounts for the distortion which depends non-linearly on the transmitted streams. Given the received signals $z_{k,t}$ and some arbitrary values of $g_{k,k'}$, it always exists a sequence $d_{k,t}$ satisfying (17). Thus, the definition of $\{g_{k,k'}\}$ and $d_{k,t}$ is ambiguous. An intuitive definition is to set $g_{k,k'}$, for all k, k' , such that they minimize the energy of the received signal, i.e.,

$$\min_{g_{k,1}, \dots, g_{k,K}} \sum_t |d_t|^2 = \min_{g_{k,1}, \dots, g_{k,K}} \sum_t \left| z_{k,t} - \sum_{k'=1}^K g_{k,k'} s_{k',t} \right|^2 \quad (18)$$

Define matrices \mathbf{G} , \mathbf{Z} and \mathbf{S} such that $[\mathbf{G}]_{k,k'} = g_{k,k'}$, $[\mathbf{Z}]_{k,t} = z_{k,t}$ and $[\mathbf{S}]_{k,t} = s_{k,t}$, respectively. Then, after some simple algebra we find that

$$\mathbf{G} = \mathbf{Z} \mathbf{S}^H (\mathbf{S} \mathbf{S}^H)^{-1}, \quad (19)$$

and at last the distortion $d_{k,t}$ can be recovered, for all users, by plugging \mathbf{G} back to (17). To assess the performance of SbS precoding, we define the signal-to-interference ratio (SIR) and the signal-to-distortion ratio (SDR) for the k -th user as:

$$\text{SIR}_k = \frac{P_s^k}{P_i^k}, \quad \text{SDR}_k = \frac{P_s^k}{P_d^k} \quad (20)$$

where

$$P_s^k = \mathbb{E} |g_{k,k} s_{k,t}|^2 = |g_{k,k}|^2 P \quad (21a)$$

$$P_i^k = \sum_{k' \neq k} \mathbb{E} |g_{k,k'} s_{k',t}|^2 = \sum_{k' \neq k} |g_{k,k'}|^2 P \quad (21b)$$

$$P_d^k = \mathbb{E} |d_{k,t}|^2 \approx \frac{1}{T} \sum_{t=1}^T |d_{k,t}|^2. \quad (21c)$$

Here, we used the fact that the transmitted streams are drawn independently from a complex Gaussian random variable $s_{k,t} \sim \mathcal{CN}(0, P)$.

IV. NUMERICAL RESULTS

Armed with Algorithms 1 to 3, we proceed to evaluate if the claim that SbS precoding can transmit more streams than RF chains in the transmitter is true. To this end, we study two antagonistic types of channels: a pure LOS channel where all users are in direct view with the BS and receive no NLOS paths, and a rich scattering channel where the channel gain between each transmit antenna and each user is an independent Gaussian-distributed random variable. For simplicity, we will further assume perfect channel state information. Unless specifically stated, the BS is equipped a uniform linear array (ULA) of 64 antennas and half-wavelength inter-antenna spacing parallel to the ground with 4 RF chains.

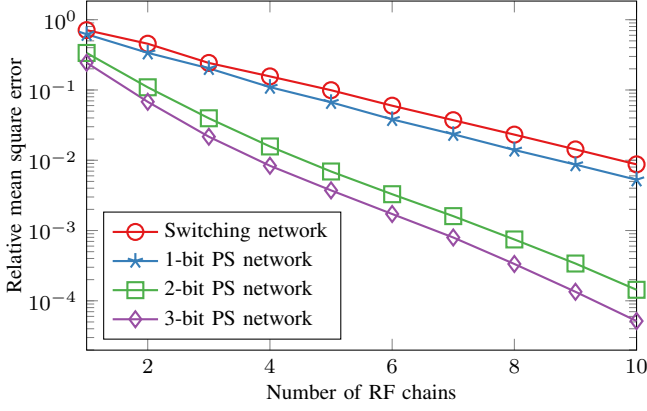


Fig. 3. Relative MSE vs. number of RF chains for the switching and phase shifting networks. The array has 64 antennas. PS stands for phase shifting.

A. Relative Mean Square Error

To assess the precision of SbS precoding in solving (8), we generate random target precoders $\mathbf{y}_t \sim \mathcal{CN}(\mathbf{0}, \mathbf{I})$ and compute the relative mean square error

$$\text{Rel. MSE} = \mathbb{E} \frac{\|\mathbf{y}_t - \hat{\mathbf{y}}_t\|_2^2}{\|\mathbf{y}_t\|_2^2}, \quad (22)$$

where \mathbb{E} is the expected value and $\hat{\mathbf{y}}_t = \mathbf{F}_{\text{RF}}^t \mathbf{f}_{\text{BB}}^t$ is an approximation obtained through Algorithms 1–3.

Fig. 3 plots the relative MSE for an increasing number of RF chains. The relative MSE decreases exponentially with the number of RF chains, and in fact with only 4 RF chains and 3-bit phase shifters, it is less than 10^{-2} . The switching and the 1-bit phase shifting networks perform the poorest, while the 2 and 3-bit phase shifting networks perform the best. Hence, the approximation (7) improves exponentially with the number of RF chains.

Fig. 4 assesses the performance of the proposed technique for different resolutions of the phase shifters. The phase shifters' resolution δ is related to the number of control bits B through the formula $\delta = 2\pi/2^B$. Unexpectedly, unless a single RF chain is used, the relative MSE is minimized when employing 3-bit phase shifters. This is a counterintuitive result because increasing the number of bits increases the phase shifters' resolution, and so theoretically speaking, we would expect better performance with finer phase shifters. This phenomenon is due to the fact that the approach based on OMP (Algorithm 1) only solves (8) exactly when employing a single RF chain, in which case we can observe that indeed the relative MSE decreases monotonically with the number of bits. In the next numerical experiments we will simulate a phase shifting hybrid architecture with 3 bits of resolution because it provides the best performance among all types of tested hybrid networks.

B. Distortion and Inter-User Interference

This experiment studies the distortion and the inter-user interference (IUI) of SbS hybrid precoding and a fully digital array for the MRT and ZF precoders in Section II-B. Simulations are performed on two different environments: a channel

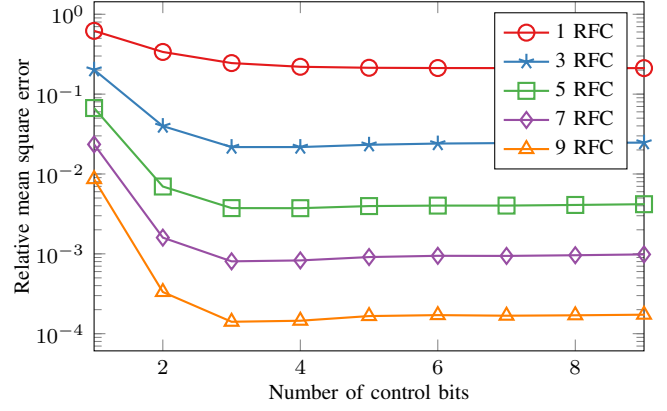


Fig. 4. Relative MSE vs. number of control bits of the phase shifters. The array has 64 antennas. RFC stands for radio-frequency chain.

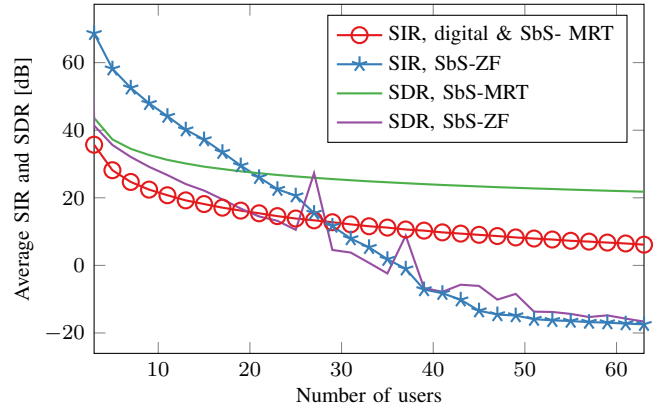


Fig. 5. Average SIR and SDR vs. number of users in LOS channels. For each channel realization, the users' azimuth are selected uniformly random between $[0, 2\pi]$, the signal strength is set equal to all users, and the phase is uniformly distributed in the interval $[0, 2\pi]$. The BS is equipped a ULA of 64 antennas.

with only the direct path between the BS and each user and a rich scattering channel.

Channels with very few paths are more common at millimeter wave frequencies than in lower frequencies, due to the higher penetration losses which greatly attenuate NLOS paths [3]. Let $\mathbf{a}(\boldsymbol{\theta})$ be array response for a signal limping from direction $\boldsymbol{\theta}$, where $\boldsymbol{\theta}$ represents the azimuth and elevation. Then, the channel matrix when all users receive the LOS path only is

$$\mathbf{H} = [\alpha_1 \mathbf{a}(\boldsymbol{\theta}_1) \quad \cdots \quad \alpha_K \mathbf{a}(\boldsymbol{\theta}_K)]^H, \quad (23)$$

where $\boldsymbol{\theta}_1, \dots, \boldsymbol{\theta}_K$ are the directions of the K users. Fig. 5 plots the SIR and SDR, averaged among all users and 1000 channel realizations, for digital MRT, digital ZF, SbS-MRT and SbS-ZF precoding. For each channel realization, the users' azimuth are selected uniformly random between $[0, 2\pi]$. Since the interest of this experiment is not to evaluate the path loss or other propagation effects, all users are assumed to have equal channel gain: $|\alpha_1| = \dots = |\alpha_K|$. Note that digital and SbS-MRT enjoy the same average SIR. For SbS-MRT, the SDR is at least 10 dB higher than the SIR, thus, the distortion introduced by SbS precoding is negligible compared to the

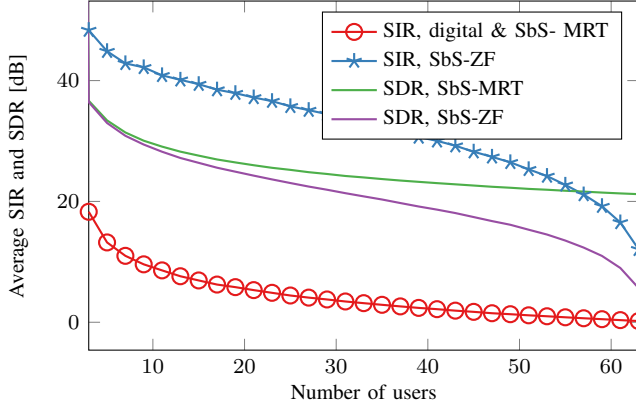


Fig. 6. Average SIR and SDR vs. number of users in NLOS channels. The channel matrix is a random Gaussian random matrix with zero-mean independent and identically distributed entries. The BS is equipped a ULA of 64 antennas.

inter-user interference (IUI). By design, digital ZF results in no IUI, however, SbS-ZF still suffers from IUI because it is an approximation of the digital ZF. The small bumps on the SDR curve of SbS-ZF are due to the fact that in a pure LOS environment with many users, the target precoding matrix \mathbf{F} suffers from numerical problems since it is obtained by inverting the MIMO channel matrix (6) which is close to singular. While not plotted here, we also studied the gain averaged users and channel realizations. For both precoding schemes, MRT and ZF, the digital and SbS implementations did not differ in gain. The gain of ZF decreased at a faster rate than that of MRT with the number of users. For example, the ZF gain was 10 dB lower than MRT gain with 20 users, and 40 dB lower with 40 users. Overall, similar to digital MRT and digital ZF, SbS-MRT outperforms SbS-ZF in terms of gain (not plotted here), SIR and SDR.

While millimeter wave MIMO is the main driver behind hybrid architectures, it is also possible to implement hybrid architectures at lower frequencies. A characteristic of the channel at few-GHz is that it is much richer in terms of multipath, and the MIMO matrix is often modeled as a Gaussian random matrix where the (k, n) -entry $h_{k,n} \sim \mathcal{CN}(0, \sigma_{\text{ch}}^2)$. Next, we repeat the same experiment but assuming a rich scattering channel. Fig. 6 plots the SIR and SDR, averaged among all users and 1000 channel realizations, for digital MRT, digital ZF, SbS-MRT and SbS-ZF precoding in a rich scattering channel. The SIR of digital and SbS- MRT goes from 20 dB for 3 users to 0 dB 63 users. In SbS-MRT the SDR is much higher than the SIR, implying that the distortion is negligible. By design, digital ZF enjoys no IUI and also no distortion. On the other hand, SbS-ZF cannot completely nullify the IUI although it is extremely mild. The limiting factor for SbS-ZF is the distortion. In this scenario, SbS-ZF outperforms digital and SbS- MRT. The average user gain was also analyzed and we found out that there is no substantial difference between the digital and SbS implementations of MRT and ZF.

When the channels are purely LOS, MRT is an attractive precoder because it has a much higher gain than ZF. From the experiments we verified that SbS-MRT has the same gain than

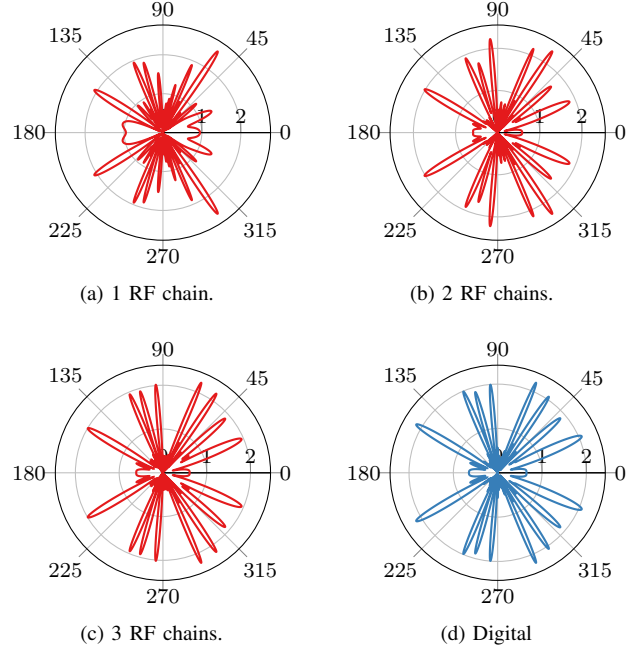


Fig. 7. In red, beam patterns produced by a 3-bit phase shifting network when serving 8 users with 1, 2 and 3 RF chains. The ULA consist of 32 antennas. In blue, the ideal target beam pattern obtained with a fully digital array which consists of multiple “pencil beams” pointing to the users.

digital MRT, and also its distortion is negligible (compared to the IUI). In rich scattering channels, MRT introduce a lot IUI, and therefore, ZF is a more attractive approach. However, contrary to digital ZF, the limiting factor in SbS-ZF was the distortion.

C. Comparison of Beam patterns

For some given weights \mathbf{y} at the antennas, the antenna gain function is defined as

$$g(\theta) = |\mathbf{a}^H(\theta)\mathbf{y}|, \quad (24)$$

where for simplicity θ only accounts for azimuth and assumes a fixed elevation. The beam pattern is a polar plot of the antenna gain for all values of θ and it is useful for visualizing how energy is irradiated at the transmitter. To showcase the potential of SbS precoding, we plot the beam patterns at a specific time instant t when serving 8 users with only 4 RF chains using a MRT precoder. The azimuths of the eight users are set to $24^\circ, 41^\circ, 56^\circ, 67^\circ, 95^\circ, 105^\circ, 113^\circ$ and 149° , and the transmitted symbols have all equal energy but random phases. To make the beam patterns more visually pleasing, the beams are enlarged by simulating a ULA with 32 antennas instead of 64. The beam pattern produced by digital MRT is also plotted in Fig. 7d and it consists, because of the large aperture, of multiple “pencil beams” pointing at each user. Figs. 7a–7c include the beam patterns of SbS-MRT with an array of 1 to 3 RF chains. Notice that visually speaking the beam pattern of SbS-MRT with only 3 RF chains is indistinguishable from that of digital MRT.

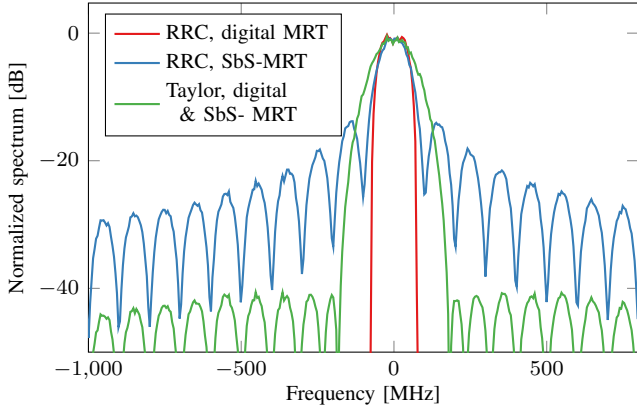


Fig. 8. Average baseband spectrum of the received signals among all users without including the noise. The symbol rate per stream is fixed to 100 Ms/s and the transmitted symbols are drawn from a complex Gaussian random variable.

D. Spectral Regrowth and Inter-symbol Interference

The phase shifters/switches operate on the continuous time-domain signal, and ideally, the phase shifts or switches should happen instantaneously in the transition of two consecutive symbols. However, in communications the symbols are usually modulated with pulses which span multiple symbols, such as the root-raised-cosine (RRC). Thus, the phase shifters/switches will introduce abrupt transitions on the signal causing two major problems: spectral regrowth, and inter-symbol interference (ISI) due to pulse distortion. A way to cope with the ISI would be to limit the duration of the pulses to a single symbol period; however, time-limited pulses are not strictly band-limited. An example is the Taylor window [35] whose spectrum has a narrow main lobe and its peak-to-side-lobe ratio is adjustable, thus avoiding ISI at the price of introducing some sidelobes. A disadvantage of using time-limited windows as pulses is that they require a large oversampling factor due to their large bandwidth (defined as width of nonzero spectral density), whereas a RRC filter occupies a bandwidth equal or smaller than twice the symbol rate. Another approach to minimizing the spectral regrowth and ISI may consist in designing a pulse with nulls strategically located at half-symbol from the pulse peak, so that when the phase shifting or switching occurs, no discontinuities are created on the transmitted signal. Nonetheless, the problem of designing an optimal pulse falls out of the scope of this paper and so will limit our analysis to pulse shaping with a RRC filter and a Taylor window.

In Fig. 8 the average spectrum of the signals received by the users (in absence of noise) is plotted when performing digital and SbS-MRT with RRC and Taylor pulse shaping. The RRC filter is set to a $\beta = 0.5$ roll-off factor and Taylor pulse is constrained to a -40 dB peak-to-side-lobe ratio in the spectrum. The number of users is fixed to $K = 30$. The spectra are estimated by transmitting 10^4 complex Gaussian random symbols for each user at a rate of 100 Ms/s. From the figure it is apparent that the spectrum generated by the digital array is band-limited, while the spectrum for the hybrid array when applying the same RRC pulse shape spills energy over a much wider range of frequencies. By using a time-limited

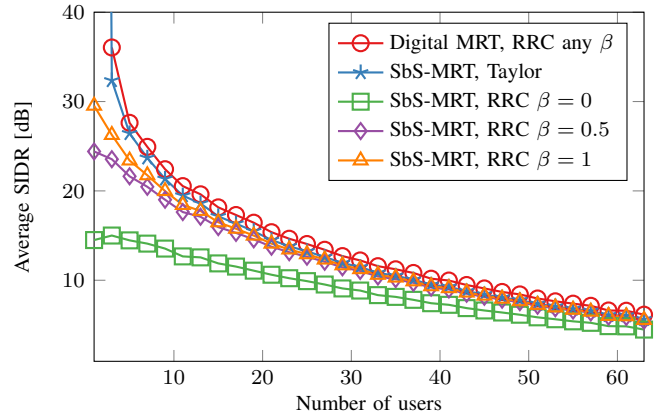


Fig. 9. Average signal-to-interference-plus-distortion ratio (SIDR) for different pulse shapes. MRT precoding over pure LOS channel. The interference accounts for user and inter-symbol interference, and the distortion is caused by the SbS hybrid precoding. The BS is equipped a ULA of 64 antennas.

Taylor pulse, we are able to approximately limit the actual bandwidth of the transmitted signal. Precisely, the -3 dB-spectrum of the received signals with RRC and Taylor pulse shaping is approximately 92 MHz and 100 MHz, respectively, while -40 dB-spectra are 150 MHz and 346 MHz. In practice, the available bandwidth would be predefined, and so the users rates for the Taylor pulse shaping would be smaller than the users rates when using a fully digital array with RRC pulse shaping.

To analyze the effect of the ISI introduced by the phase shifters/switches, Fig. 9 plots the average signal-to-interference-plus-distortion ratio (SIDR) when using different pulse shapes. Here, interference encompasses IUI and ISI. The channel is a pure LOS with every user and the transmission scheme is SbS-MRT. In digital MRT no ISI appears (because of the RRC pulse shape) nor distortion (because it is digital), thus, the only term appearing in denominator of the SIDR is the IUI. The SIDR in SbS-MRT with Taylor pulse shaping is slightly worse than digital MRT due to the distortion; however, no ISI is aggregated because the Taylor pulse is time-limited to a symbol period. When SbS-MRT hybrid precoding with a RRC pulse with a roll-off factor of $\beta = 0.5$ and $\beta = 1$, the SIDR is slightly degraded compared to Taylor pulse shape because of the ISI. Nonetheless, except for the case where the RRC roll-off factor is $\beta = 0$, in general all other schemes perform similarly for 10 or more users due to the fact that IUI, which is the most limiting factor, affects them all more or less equally. The pulse shape of the RRC with $\beta = 0$ corresponds to a ‘sinc’ pulse shape, and as such it is more heavily affected by ISI.

The simulation setup of Fig. 10 is the same than in Fig. 9 except for the fact that we simulate a rich scattering channel and the BS uses ZF precoding. Digital ZF enjoys no IUI, no ISI because (because of the RRC pulse shape) and no distortion (because it is digital). Consequently the SIDR of digital ZF is infinite and not shown in the plot. Aside from digital ZF, SbS-ZF with a Taylor pulse performs the best as it is ISI free. Similar to the experiment of Fig. 9, SbS-ZF with RRC is best with a roll-off factor of $\beta = 1$ and worst

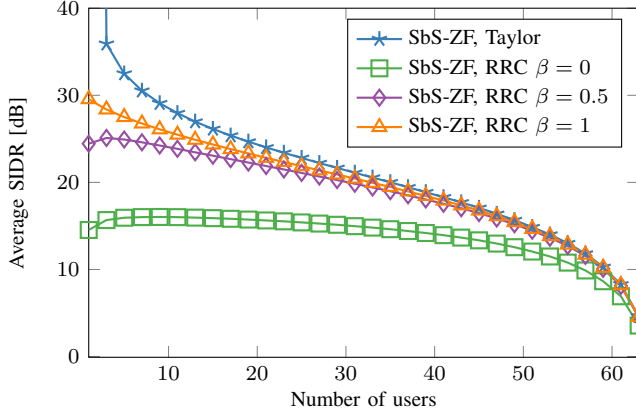


Fig. 10. Average signal-to-interference-plus-distortion ratio (SIDR) for different pulse shapes. ZF precoding over rich scattering channel. The interference accounts for user and inter-symbol interference, and the distortion is caused by the SbS hybrid precoding. The BS is equipped a ULA of 64 antennas.

with $\beta = 0$. In general, in both setups, SbS hybrid precoding performs the best when using a time-limited pulse. However, the degradation due to ISI when using a RRC filter with a roll-off factor $\beta \geq 0.5$ is small.

E. Sum-Rate Analysis

We expect that thanks to serving more users, SbS hybrid precoding also achieves higher sum-rates than standard hybrid precoding which is limited by the number of RF chains. Since users do not cooperate between them, the IUI is treated as Gaussian noise, and we also make the simplifying assumption that the distortion is Gaussian. For user k , the maximum achievable rate is given by Shannon's capacity formula

$$C_k = R_k \log_2 (1 + \text{SINDR}_k) \quad (25)$$

where R_k is the symbol rate of the k -th stream and the SINDR (signal-to-interference-noise-and-distortion ratio) is defined as

$$\text{SINDR}_k = \frac{P_s^k}{P_n + P_i^k + P_d^k}. \quad (26)$$

The powers P_s^k , P_i^k and P_d^k were defined in (21), and P_n is the noise variance which for simplicity is assumed equal for all users.

Fig. 11 plots the achievable sum-rate normalized by the signal bandwidth, averaged among 1000 channel realizations, for digital MRT, standard hybrid MRT and SbS-MRT, in a pure LOS channel. By standard hybrid MRT we refer to the strategy where the analog and digital precoding matrices are fixed during the entire transmission of the streams (4), and the analog precoder is populated with the steering vectors of the first L users (where L is the number of RF chains) $\mathbf{F}_{\text{RF}} = [\mathbf{a}(\theta_1), \dots, \mathbf{a}(\theta_L)]$, whereas the digital precoder \mathbf{F}_{BB} is set to the identity matrix. Since the entries of \mathbf{F}_{RF} are limited to discrete phase shifts, the best least squares approximation can be retrieved by Algorithm 2. Digital and standard hybrid MRT use RRC pulse shaping whereas SbS-MRT employs the Taylor window. The bandwidth available to the BS is fixed to 100 MHz and a constraint on the peak-to-side-lobe ratio of

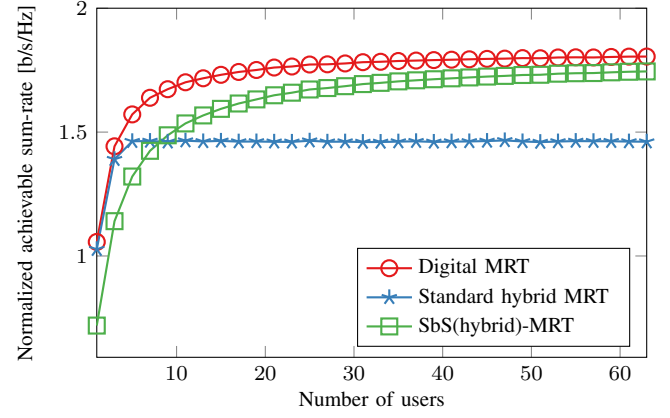


Fig. 11. Normalized achievable sum-rate averaged over 1000 channel realizations. For each channel realization, the users' azimuth are selected uniformly random between $[0, 2\pi]$, the signal strength is set equal to all users, and the phase is uniformly distributed in the interval $[0, 2\pi]$. The BS is equipped a ULA of 64 antennas. BS is using a MRT precoder.

−40 dB. To this end the symbol rates are adjusted in order to meet the bandwidth specification. The total transmit power at the BS and the noise power at the receivers are set so that, when serving a single user with digital MRT, the signal-to-noise ratio (SNR) is 20 dB. For the case of more than 1 user, the power is distributed evenly. Thus, the SNR never exceeds 20 dB, and in fact it decreases rapidly with the number of users.

From Fig. 11, as expected digital MRT delivers the highest sum-rate for any number of users. When the number of users is less or equal to the number of RF chains (4 in our set-up), standard hybrid MRT performs just as well because the MRT precoding matrix (5),(23) is well approximated with the hybrid phase shifting network. However, we can observe in Fig. 11 that the sum-rate saturates to a constant value when the number of users exceeds the number of RF chains $K > L$ because, as explained in Section II-A, the number of actual users served is capped by the number of RF chains. For $K \leq L$, SbS-MRT performs worse than standard hybrid MRT because it uses the Taylor phase shifting network as a pulse which offers a slower symbol rate for the same bandwidth than RRC. However, as the number of users increases, SbS-MRT outperforms standard hybrid MRT because it serves more users, and due to the slower symbol rate the energy per symbol is higher. Ideally, for a small number of users, we would perform standard hybrid MRT precoding and then switch to SbS-MRT for large number of users.

V. CONCLUSIONS

Arrays with hybrid analog-digital precoding capabilities are an attractive solution for implementing massive MU-MIMO at mm-Wave. However, an inherent limitation is that the number of users served by the BS is limited by the number of RF chains. We have proposed a novel precoding strategy for fully meshed hybrid arrays of phase shifters or switches, which enables serving more users than RF chains in the same time-frequency slot. The strategy changes on a symbol-by-symbol (SbS) basis the precoding matrices, which are computed based on an exact and novel solution to orthogonal matching pursuit.

We show that in the proposed strategy (i) the approximation error decreases exponentially with the number of RF chains (ii) hybrid 3-bit phase shifting network are optimal, even when compared to infinite-resolution phase shifters; (iii) there are negligible distortions of the transmitted streams when combined with MRT precoding; (iv) spectral regrowth caused by performing ultra-fast phase shifting or switching can be combated through appropriate pulse shaping.

REFERENCES

- [1] E. G. Larsson, O. Edfors, F. Tufvesson, and T. Marzetta, "Massive MIMO for next generation wireless systems," *IEEE Communications Magazine*, vol. 52, no. 2, pp. 186–195, 2014.
- [2] J. G. Andrews, S. Buzzi, W. Choi, S. V. Hanly, A. Lozano, A. C. Soong, and J. C. Zhang, "What will 5G be?" *IEEE Journal on selected areas in communications*, vol. 32, no. 6, pp. 1065–1082, 2014.
- [3] T. S. Rappaport, S. Sun, R. Mayzus, H. Zhao, Y. Azar, K. Wang, G. N. Wong, J. K. Schulz, M. Samimi, and F. Gutierrez, "Millimeter wave mobile communications for 5G cellular: It will work!" *IEEE Access*, vol. 1, pp. 335–349, May 2013.
- [4] P. Wang, Y. Li, L. Song, and B. Vucetic, "Multi-gigabit millimeter wave wireless communications for 5G: From fixed access to cellular networks," *IEEE Communications Magazine*, vol. 53, no. 1, pp. 168–178, 2015.
- [5] S. Han, I. Chih-Lin, Z. Xu, and C. Rowell, "Large-scale antenna systems with hybrid analog and digital beamforming for millimeter wave 5G," *IEEE Communications Magazine*, vol. 53, no. 1, pp. 186–194, 2015.
- [6] R. Méndez-Rial, C. Rusu, N. González-Prelcic, A. Alkhateeb, and R. W. Heath, "Hybrid mimo architectures for millimeter wave communications: Phase shifters or switches?" *IEEE Access*, vol. 4, pp. 247–267, 2016.
- [7] J. Brady, N. Behdad, and A. M. Sayeed, "Beamspace MIMO for millimeter-wave communications: System architecture, modeling, analysis, and measurements," *IEEE Transactions on Antennas and Propagation*, vol. 61, no. 7, pp. 3814–3827, 2013.
- [8] A. Alkhateeb, J. Mo, N. Gonzalez-Prelcic, and R. W. Heath, "MIMO precoding and combining solutions for millimeter-wave systems," *IEEE Communications Magazine*, vol. 52, no. 12, pp. 122–131, 2014.
- [9] Z. Gao, L. Dai, D. Mi, Z. Wang, M. A. Imran, and M. Z. Shaker, "MmWave massive-MIMO-based wireless backhaul for the 5G ultra-dense network," *IEEE Wireless Communications*, vol. 22, no. 5, pp. 13–21, 2015.
- [10] R. W. Heath, N. Gonzalez-Prelcic, S. Rangan, W. Roh, and A. M. Sayeed, "An overview of signal processing techniques for millimeter wave MIMO systems," *IEEE journal of selected topics in signal processing*, vol. 10, no. 3, pp. 436–453, 2016.
- [11] T. E. Bogale and L. B. Le, "Beamforming for multiuser massive MIMO systems: Digital versus hybrid analog-digital," in *Global Communications Conference (GLOBECOM)*. IEEE, 2014, pp. 4066–4071.
- [12] R. Bonjour, M. Singleton, S. A. Gebrewold, Y. Salamin, F. C. Abrecht, B. Baeuerle, A. Josten, P. Leuchtmann, C. Hafner, and J. Leuthold, "Ultra-fast millimeter wave beam steering," *IEEE Journal of Quantum Electronics*, vol. 52, no. 1, pp. 1–8, 2016.
- [13] L. He, J. Wang, and J. Song, "Spatial modulation for more spatial multiplexing: RF-chain-limited generalized spatial modulation aided mmWave MIMO with hybrid precoding," *arXiv preprint arXiv:1709.02528*, 2017.
- [14] V. Venkateswaran and A.-J. van der Veen, "Analog beamforming in MIMO communications with phase shift networks and online channel estimation," *IEEE Transactions on Signal Processing*, vol. 58, no. 8, pp. 4131–4143, 2010.
- [15] O. El Ayach, R. W. Heath, S. Abu-Surra, S. Rajagopal, and Z. Pi, "Low complexity precoding for large millimeter wave mimo systems," in *IEEE International Conference on Communications*. IEEE, 2012, pp. 3724–3729.
- [16] A. Alkhateeb, O. El Ayach, G. Leus, and R. W. Heath, "Hybrid precoding for millimeter wave cellular systems with partial channel knowledge," in *IEEE Information Theory and Applications Workshop*, 2013, pp. 1–5.
- [17] D. De Donno, J. P. Beltrán, D. Giustiniano, and J. Widmer, "Hybrid analog-digital beam training for mmWave systems with low-resolution RF phase shifters," in *IEEE International Conference on Communications Workshops*, 2016, pp. 700–705.
- [18] O. El Ayach, R. W. Heath, S. Rajagopal, and Z. Pi, "Multimode precoding in millimeter wave MIMO transmitters with multiple antenna sub-arrays," in *Global Communications Conference*. IEEE, 2013, pp. 3476–3480.
- [19] S. Park, A. Alkhateeb, and R. W. Heath, "Dynamic subarrays for hybrid precoding in wideband mmwave MIMO systems," *IEEE Transactions on Wireless Communications*, vol. 16, no. 5, pp. 2907–2920, 2017.
- [20] R. Méndez-Rial, C. Rusu, N. González-Prelcic, and R. W. Heath, "Dictionary-free hybrid precoders and combiners for mmwave MIMO systems," in *16th International Workshop on Signal Processing Advances in Wireless Communications*. IEEE, 2015, pp. 151–155.
- [21] A. Alkhateeb, G. Leus, and R. W. Heath, "Limited feedback hybrid precoding for multi-user millimeter wave systems," *IEEE transactions on wireless communications*, vol. 14, no. 11, pp. 6481–6494, 2015.
- [22] V. Selvan, M. Iqbal, and H. Al-Raweshidy, "Performance analysis of linear precoding schemes for very large multi-user MIMO downlink system," in *Fourth International Conference on Innovative Computing Technology*. IEEE, 2014, pp. 219–224.
- [23] J. Lee and N. Jindal, "High SNR analysis for MIMO broadcast channels: Dirty paper coding versus linear precoding," *IEEE Transactions on Information Theory*, vol. 53, no. 12, pp. 4787–4792, 2007.
- [24] C. B. Peel, B. M. Hochwald, and A. L. Swindlehurst, "A vector-perturbation technique for near-capacity multiantenna multiuser communication-part I: channel inversion and regularization," *IEEE Transactions on Communications*, vol. 53, no. 1, pp. 195–202, 2005.
- [25] M. Uzunkol and G. M. Rebeiz, "A 65 GHz LNA/phase shifter with 4.3 dB NF using 45 nm CMOS SOI," *IEEE Microwave and Wireless Components Letters*, vol. 22, no. 10, pp. 530–532, 2012.
- [26] W.-T. Li, Y.-C. Chiang, J.-H. Tsai, H.-Y. Yang, J.-H. Cheng, and T.-W. Huang, "60-GHz 5-bit phase shifter with integrated VGA phase-error compensation," *IEEE Transactions on Microwave Theory and Techniques*, vol. 61, no. 3, pp. 1224–1235, 2013.
- [27] F. Meng, K. Ma, K. S. Yeo, S. Xu, C. C. Boon, and W. M. Lim, "Miniaturized 3-bit phase shifter for 60 GHz phased-array in 65 nm CMOS technology," *IEEE Microwave and Wireless Components Letters*, vol. 24, no. 1, pp. 50–52, 2014.
- [28] R. L. Schmid, P. Song, C. T. Coen, A. Ç. Ulusoy, and J. D. Cressler, "On the analysis and design of low-loss single-pole double-throw W-band switches utilizing saturated SiGe HBTs," *IEEE Transactions on Microwave Theory and Techniques*, vol. 62, no. 11, pp. 2755–2767, 2014.
- [29] A. Alkhateeb, O. El Ayach, G. Leus, and R. W. Heath, "Channel estimation and hybrid precoding for millimeter wave cellular systems," *IEEE Journal of Selected Topics in Signal Processing*, vol. 8, no. 5, pp. 831–846, 2014.
- [30] J. Mirza, B. Ali, S. S. Naqvi, and S. Saleem, "Hybrid precoding via successive refinement for millimeter wave MIMO communication systems," *IEEE Communications Letters*, 2017.
- [31] J. A. Tropp and A. C. Gilbert, "Signal recovery from random measurements via orthogonal matching pursuit," *IEEE Transactions on information theory*, vol. 53, no. 12, pp. 4655–4666, 2007.
- [32] B. L. Sturm, M. Græsb *et al.*, "Comparison of orthogonal matching pursuit implementations," in *20th European Signal Processing Conference (EUSIPCO)*. IEEE, 2012, pp. 220–224.
- [33] K. Mackenthun, "A fast algorithm for multiple-symbol differential detection of MPSK," *IEEE Transactions on Communications*, vol. 42, no. 234, pp. 1471–1474, 1994.
- [34] W. Sweldens, "Fast block noncoherent decoding," *IEEE communications letters*, vol. 5, no. 4, pp. 132–134, 2001.
- [35] D. C. Rife and G. Vincent, "Use of the discrete Fourier transform in the measurement of frequencies and levels of tones," *Bell Labs Technical Journal*, vol. 49, no. 2, pp. 197–228, 1970.